

RESEARCH

Open Access



A RSBU-LSTM network for radio frequency fingerprint identification relying on multiple features

Haoran Ling^{1*} ID, Fengchao Zhu^{1†} and Minli Yao^{1†}

¹Fengchao Zhu, Minli Yao have contributed equally to this work.

*Correspondence:
15009176717@163.com

¹ PLA Rocket Force University of Engineering, Xi'an 710025, China

Abstract

Radio frequency fingerprint identification (RFFI) can distinguish highly similar wireless communication devices to protect physical layer security and improve the security of wireless networks effectively, which has been widely used for spectrum management and physical layer secure communication. However, most RFFI methods show a degradation of performance under low signal-to-noise ratio (SNR) environments. In this paper, we propose a RSBU-LSTM network relying on multiple features to improve the identification accuracy with low SNR. Firstly, we use multiple features of in-phase (I), quadrature (Q), and phase as inputs. Then, we use multiple Residual Shrinkage Building Units (RSBUs) to extract the correlation features within the cycle of signals and preserve as many features as possible in low SNR environments. Finally, we use the long short-term memory (LSTM) to extract the relevant features of the signals of non-adjacent cycles. The experimental results show that the proposed network can effectively complete RFFI in low SNR environments and show better performance than other models used for comparison.

Keywords: Physical layer security, Radio frequency fingerprint identification, Deep learning, Residual shrinkage building units, Long short-term memory

1 Introduction

With the development of new generation wireless communication technology and Internet of Things (IoT) technology represented by 5 G, human society has entered an era of information and intelligence where everything is interconnected. As the IoT has been widely used in smart cities, smart grids, industrial Internet, and other fields, the research on IoT technology is increasing [1]. According to predictions, the number of IoT devices worldwide will reach 25.2 billion by 2025, and the annual revenue of IoT suppliers selling IoT hardware, software, and comprehensive solutions may exceed 470 billion dollars [2]. However, the openness of radio waves has led to many illegal access and hacker attacks, which can easily cause property and mental damage to people. The key of solving this problem is to quickly identify illegal wireless individuals attempting to deceive or invade the network through wireless individual identification. Fortunately, there are subtle differences in the electronic device parameters inside each signal transmitter, which

is inevitable in the manufacturing of electronic devices. Therefore, each device has its unique hardware features that are difficult to tamper with or forge. These unique features are called radio frequency fingerprints (RFFs). Radio frequency fingerprint identification (RFFI) has been widely used for spectrum management and physical layer secure communication [3].

Traditional RFFI methods mostly extract physical parameter features of signals in the time domain or transform domain. After obtaining features, individual identification of radiation sources is accomplished through a classifier. In terms of feature extraction, fast Fourier transform [4], short-time Fourier transform [5], and discrete Gabor transform [6, 7] were frequently adopted. Classic machine learning classifiers, including support vector machines (SVM) [8, 9] and random forests [10, 11], are used to identify signal transmitters using these different time–frequency features. Based on this, reference [12] proposed an RFFs extraction and device identification algorithm based on multiscale fractal features and SVM, the proposed model achieving an average identification accuracy of 99.13% for 16 Bluetooth devices. Reference [13] investigated the impact of the usage of carrier frequency offset (CFO) on RFFI accuracy, and it can be used for identification when they are relatively distinguishable. In addition, new unsupervised machine learning (ML) [14] algorithms have also been applied in RFFI. Unfortunately, these traditional feature engineering-based identification methods mostly rely on experiential design of RFF features and prior knowledge of signals, resulting in a lack of universality and poor real-time performance, which cannot meet current practical needs.

As deep learning demonstrates its powerful feature extraction capability, it has gradually been applied to RFFI [15]. In order to fully leverage the significant advantages of convolution neural network (CNN) in processing image data, differential constellation diagram [16], compressed time–frequency spectrum [17], double layer waveform domain image [18], constellation trajectory [19], bimodal feature map [20], and other images were used as inputs. Due to the loss of some information during the process of converting to images, the accuracy of identification is affected. Therefore, lots of innovative neural network models have been appeared. Reference [21] proposed the Adaptive Radio Frequency Fingerprint Fusion Network (ARFNet) which can extract and adaptively fuse multiple RFFs in a data-driven manner and achieved high identification accuracy. Reference [22] proposed a RFFID method based on lightweight CNN, and the result shows that this method can identify Zigbee device, and the accuracy reached 100%. In addition, long short-term deep neural network (CLDNN) [23], dense neural network (DNN) [24], multi-scale convolutional neural network (MSCNN) [25], slice combination CNN [26] are also good models to complete RFFI. Similarly, reference [27, 28] combining machine learning classifiers with neural networks also improved identification accuracy. With the rapid development of artificial intelligence (AI), generative adversarial network (GAN) [29], transfer learning [30, 31], incremental learning [32], meta-learning [33], federated learning [34], and other methods have gradually been applied in RFFI.

According to research findings, many models experience a decrease in identification performance under non-ideal environmental conditions such as low signal-to-noise ratio (SNR). Reference [35] proposed an intelligent signal processing method against noise interference that draws on the concept of the CNN. Reference [36] proposed a dynamic shrinkage learning network (DSLN) to improve identification accuracy in low SNR environments

by utilizing dynamic shrinkage thresholds. Inspired by these, we propose a new network to address this issue in this paper. In order to extract RFFs to the maximum extent possible, we first consider using multiple features including in-phase (I), quadrature (Q), and phase as inputs to the network. Then, we use multiple Residual Shrinkage Building Units (RSBUs) to suppress noise and extract the correlation features. At the same time, we use the long short-term memory (LSTM) to extract the relevant features of the signals of non-adjacent cycles. Finally, concatenate the features of sub-networks and obtain prediction results through the fully connect (FC) layer. The main contributions are as follows:

- (1) Different from previous works that directly input signals into the network, we consider not only the real and imaginary part information of the signal, but also its phase information in the signal processing stage. Due to the fact that phase information also includes the RFFs of the signal, the proposed signal input is more comprehensive.
- (2) Different from directly inputting data into CNN [37] for feature extraction, we use RSBUs for feature extraction, introducing soft thresholding to reduce the impact of noise on feature extraction and better extraction of relevant features within and between adjacent cycles.
- (3) Different from previous works that directly output prediction results after using CNN feature extraction, we use LSTM network to extract the relevant features of the signals of non-aggressive cycles. And all the extracted features were concatenated to achieve diversity in feature extraction.
- (4) To test the progressiveness of the proposed network, we conducted simulation experiments and compared the network with the one-dimensional CNN (1D-CNN)-based method and its improved version. The results indicate that our network can achieve better identification accuracy under low SNR conditions.

The rest of this paper is organized as follows: Specific methods are explained in Sect. 2. In Sect. 3, experimental design is described. In Sect. 4, results and discussion are presented. The conclusion and future work are shown in Sect. 5.

2 Signal model and the RSBU-LSTM network

In this section, we propose a method for extracting signal features, the components of the network model, and a complete network model.

2.1 Signal model and feature extraction

Consider the RF signal $s(t)$ is expressed as:

$$s(t) = w(t) + n(t) \quad (1)$$

where $w(t)$ is the signal carrying information and $n(t)$ is noise. The intercepted signal is expressed as:

$$r(t) = s_r(t)e^{j2\pi f_0' t} = s_r(t)(\cos(2\pi f_0' t) + j \sin(2\pi f_0' t)) \quad (2)$$

where $r(t)$ represents received signal and f_0' is the estimated carrier frequency. Use orthogonal carriers to obtain complex signal $r_c(t)$:

$$r_c(t) = I(t) + jQ(t) \quad (3)$$

In order to obtain more signal features, we extract $I(t)$, $Q(t)$, and $P(t)$ three types of data.

$$I(t) = r(t) \cos(2\pi f_0' t) \quad (4)$$

$$Q(t) = r(t) \sin(2\pi f_0' t) \quad (5)$$

$$P(t) = \arctan(Q(t)/I(t)) \quad (6)$$

2.2 Residual shrinkage building unit (RSBU)

When facing a large amount of high noise signals, deep residual networks (ResNet) using convolutional kernels as local feature extractors may not be able to detect RFFs, resulting in poor discriminative power of high-level features learned by the output layer, which is insufficient to achieve accurate device identification. RSBU [38] combines the characteristics of ResNet's identical cross-layer connections, improves the stability and training efficiency of deep learning models, and introduces soft thresholding and attention mechanisms, which can effectively overcome the shortcomings of feature extraction difficulties in convolutional kernels. The structure of RSBU is shown in Fig. 1.

We input all the three types of data into the RSBU module. Assume $I(t) = x$, $Q(t) = y$, and $P(t) = z$. We take signal sequence x as an example. In RSBU, features are first divided into two paths, one path entering two convolutional layers for feature refinement. Each convolutional layer is accompanied by batch normalization (BN) and ReLU operations.

$$x_j^k = f \left(\sum_{N=1}^{i=1} x_i^{k-1} * w_{ij}^k + b_j^k \right) \quad (7)$$

$$f(x) = (0, x) \quad (8)$$

Vector x_i^{k-1} is the i th feature vector of the previous $(k-1)$ th layer, x_j^k is the j th feature vector of the current k th layer, and N is the number of input feature vectors. w_{ij}^k and b_j^k represent the weight and bias of the neuron, respectively. $*$ is the convolution operation, and $f(x)$ is a rectified linear unit (ReLU), which can increase the nonlinear expression ability. After these two layers of convolution, the obtained feature x is first subjected to

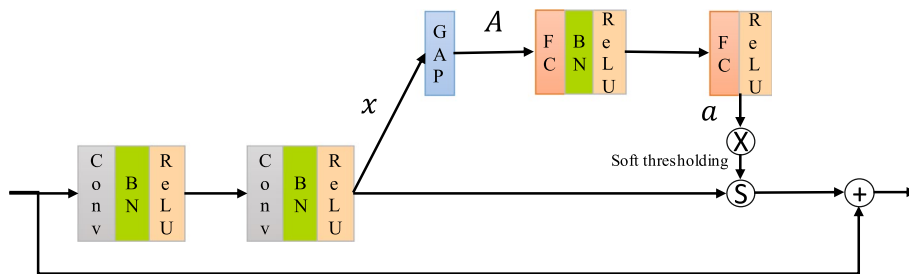


Fig. 1 The structure of RSBU

absolute value processing and then reduced to a one-dimensional vector through global average pooling (GAP). Finally, feature A is obtained, represented as:

$$A = \text{average}|x_{i,j,c}| \quad (9)$$

where i , j , and c are the width, height, and channel indices of feature x , respectively. This one-dimensional vector is divided into two paths. All inputs are fed into the attention mechanism module composed of two FC layers, where the first FC layer contains BN and ReLU, while the second FC layer only has ReLU. The number of output neurons in this module matches the number of input feature channels. Normalizing the output between 0 and 1 is represented as,

$$\alpha_c = \frac{1}{1 + \exp(-Z_c)} \quad (10)$$

where Z_c is a neuron, and α is its corresponding scaling parameter. The average value of the other channel is multiplied by the output of the attention module to obtain the exclusive threshold for each channel.

$$\tau_c = \alpha_c \times A \quad (11)$$

where τ_c is the threshold of channel c for feature x . Using the results obtained above, after performing a soft thresholding operation, it is added to the original segmented features to achieve cross-layer identity connections.

$$M = m + \tau_c \times m, (M = X, Y, Z; m = x, y, z) \quad (12)$$

M is the output of RSBU and also the input of the next RSBU. X , Y , and Z represent the outputs of the I-channel characteristics x , Q-channel characteristics y , and phase characteristics z input into RSBU, and they are also the inputs of the next RSBU.

After going through multiple layers of RSBU, these three features are respectively input into three LSTMs.

2.3 Long short-term memory (LSTM)

LSTM [39] is a variant of recurrent neural networks (RNN) which is used for processing a sequence of data. Compared with classical RNN, it can effectively capture the correlation information between temporal data and alleviate gradient vanishing or exploding phenomena. It uses hidden memory information instead of ordinary hidden nodes and has higher sensitivity to time series data. Its core structure consists of four parts: forget gate, input gate, cell state, and output gate. The structure of LSTM is shown in Fig. 2.

The hidden state and cell output are denoted by h_t and c_t , respectively. x_t represents the current sequence input. In this implementation, LSTM is formulated as:

$$f_t = \sigma(W_f \cdot [h_{t-1}, x_t] + b_f) \quad (13)$$

$$i_t = \sigma(W_i \cdot [h_{t-1}, x_t] + b_i) \quad (14)$$

$$o_t = \sigma(W_o \cdot [h_{t-1}, x_t] + b_o) \quad (15)$$

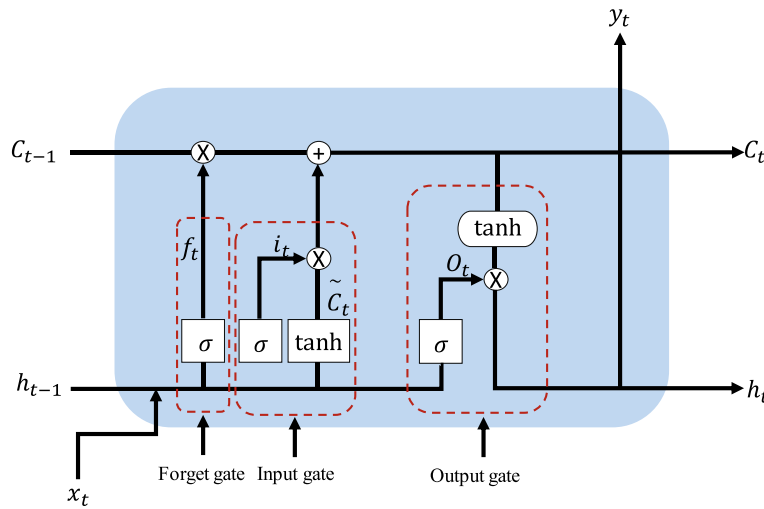


Fig. 2 The structure of LSTM

$$\tilde{c}_t = \tanh(W_c \cdot [h_{t-1}, x_t] + b_c) \quad (16)$$

$$c_t = f_t \odot c_{t-1} + i_t \odot \tilde{c}_t \quad (17)$$

$$h_t = o_t \odot \tanh(c_t) \quad (18)$$

In the equations above, f_t , i_t , \tilde{c}_t , o_t are the input, forget, cell, and output gates, respectively. W_f , W_i , and W_o represent the weight matrix of forget gate, input gate, and output gate, respectively. b_f , b_i , and b_o represent the deviation of the forget gate, input gate, and output gate, respectively. c_{t-1} and h_{t-1} represent the state of the memory layer and the hidden layer at the previous moment, respectively. σ is the sigmoid function. \tanh is the hyperbolic tangent activation function. \cdot denotes the convolutional operator, and \odot is the Hadamard function. According to this formula, both hidden and cell states in the previous block are used for the calculation of these states in each block.

Then, we concatenate the outputs of three LSTMs.

$$M = \text{concat}(x(h_t, c_t), y(h_t, c_t), z(h_t, c_t)) \quad (19)$$

M represents the features after concatenating. Finally, we use the FC layer to complete device prediction and identification.

Overall, Fig. 3 shows a general overview of the RSBU-LSTM network relying on multiple features. For the input of the network, it is fed with three channel signals of I, Q, and phase. Then after a convolution, the signal is fed into the RSBU. To maximize the preservation of RFFs in low SNR environments. Finally, the relevant features of the non-adjacent periods of the signal are further extracted through LSTM. In order to fully utilize various information and improve identification accuracy, all features are connected together to obtain more robust features. At the same time, establish the output of the layer corresponding to the individual device, and use the FC layer to achieve the identification of individual devices.

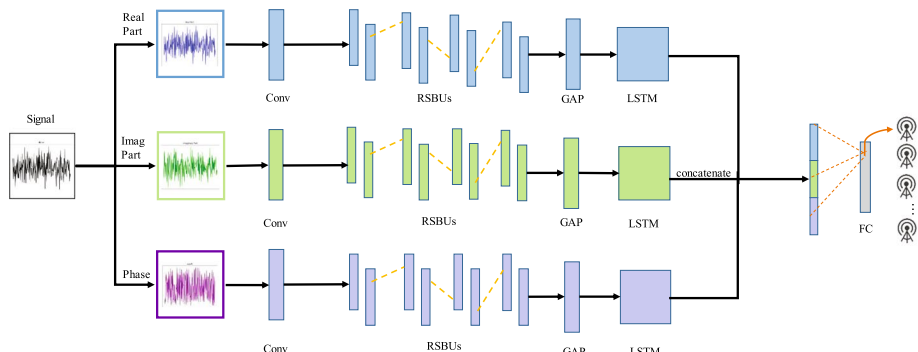


Fig. 3 Illustration of the RSBU-LSTM network relying on multiple features

3 Experimental design

In this section, we introduced the dataset and data processing used for the experiment, the experimental environment, and the experimental training strategy.

3.1 Simulation data

In order to test the effectiveness of RSBU-LSTM network under complex noise environment, we use the open dataset, referred to as KRI-16IQImbalances [40]. This is a dataset collected from an experimental setup of USRP SDR with a fixed USRP B210 as the receiver. All 16 transmitters are bit-similar USRP X310 radios that emit IEEE 802.11a standards compliant frames generated via a MATLAB WLAN System toolbox. The data frames generated contain random payload but have the same address fields and are then streamed to the selected SDR for over-the-air wireless transmission and the transmitter–receiver distance is 62 feet. The receiver SDR samples the incoming signals at 5 MS/s sampling rate at center frequency of 2.45 GHz. The collected signals are processed into raw I/Q sequences through IQ balance compensation and DC offset compensation. Overall, they collected approximately 2 million sampling points for each radio. We extracted 500 samples from the signal of each radio, each containing 2560 points. The experimental data accounts for approximately 60% of the dataset. Assuming that a signal sample is $x(n)$, the signal power of this sample can be expressed as:

$$P_n = \frac{1}{N} \sum_{n=0}^{N-1} |x[n]|^2 \quad (20)$$

P_n represents the signal power of this sample. N is the length of the sample signal. To add Gaussian white noise of -5dB $\sim 20\text{dB}$, we calculated the corresponding noise power P_s .

$$P_s = \frac{P_n}{10^{\frac{a}{10}}}, a = [-5, 0, 5, 10, 15, 20] \quad (21)$$

a is the specified value of the SNR. Then, we can generate Gaussian random variables with zero mean and appropriate variance (variance equal to noise power) to simulate Gaussian white noise. Once we have a noisy signal, we can add it to the original signal.

$$y[n] = x[n] + n[n] \quad (22)$$

$y[n]$ represents the signal with Gaussian white noise, and $n[n]$ represents the noise. The processing sample signals are divided into the training set and test set in a ratio of 8:2. The training set is applied to train the network model; the test set is applied to assess the property of the network model.

3.2 Experimental environment

In terms of hardware for the experimental environment, the CPU is Intel Xeon Sliver 4210R, the memory is 32GB, the hard disk is 512 G SSD, and the GPU is GeForce RTX 3090. In terms of software, design, development, training, and testing are based on Python 3.10 and the deep learning framework Python 1.12.1. In addition, both the model and data are loaded into the GPU and accelerated through CUDA technology.

3.3 Training design

In the training phase, cross-entropy was chosen as the loss function, and the parameters were optimized using the SGD algorithm. The elementary learning rate was set to 0.01, and it was set to 0.001 for 20 iterations, for a total of 100 iterations. Each iteration shuffles the training samples and sets the batch size to 16 to speed up the learning of model parameters. The hyper-parameter configuration for model training is shown in Table 1.

4 Simulation results

In this section, we first tested the effectiveness of extracting multiple features, then verified the necessity of each part of the network through ablation experiments, and finally compared the performance with several similar networks, proving the progressiveness nature of the proposed network.

4.1 Feature extraction effectiveness and analysis

In the experiment, the proposed network using two channel data and the same network using three channel data are selected for comparison. Figure 4 shows the average identification accuracy of 16 devices signals for the proposed network using two channel data and three channel data.

From Fig. 4, it can be seen that the average identification accuracy of the four networks increases with the increase in SNR. When the SNR is $-5\text{dB} \sim 20\text{dB}$, the average identification accuracy of the network using three channel data is higher than that of

Table 1 Hyper-parameter configuration

Hyper-parameter	Parameter value
Epoch	100
Batch-size	16
Optimizer	SGD
Initial learning rate	0.01
Weight-Decay	0.0005
Momentum	0.9
Num-Print	100

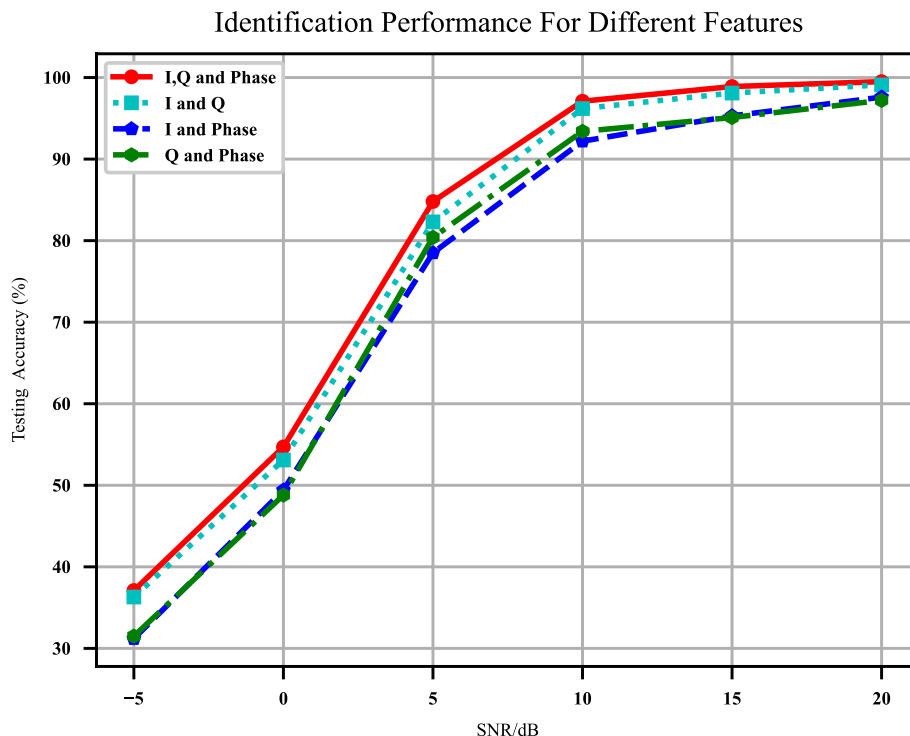


Fig. 4 Identification performance for different features

the network model using any two channel data. The identification accuracy of the network using three channel data is significantly improved compared to other network models when the SNR is $-5\text{dB} \sim 5\text{dB}$, with an average identification accuracy of 58.9%. Compared to using I-channel data and Q-channel data, I-channel data and phase data, Q-channel data and phase data increased by 1.7%, 5.8%, and 5.3%, respectively. Based on the above analysis, it can be concluded that using multiple features can improve identification accuracy, which verifies the rationality of the feature extraction algorithm in this paper.

4.2 Ablation experiment and analysis

To evaluate each part of the proposed network, the RSBUs using three channel data and LSTM using three channel data are selected for comparison. The ablation experimental results are shown in Fig. 5. Case 1 represents the network lack of LSTM, directly concatenating the output of RSBUs and obtaining prediction results through FC layer. Case 2 represents the network lack of RSBUs, input the three channel data into basic residual blocks and LSTM, concatenating all features and then outputting prediction results through the FC layer.

It can be seen from Fig. 5 that Case 1 and Case 2 show a significant decrease in identification accuracy compared to the original network when the SNR is $-5\text{dB} \sim 20\text{dB}$. As the SNR increases, the RFF carried in the signal becomes more significant. And the identification accuracy of Case1 is always higher than Case2 when the SNR is $-5\text{dB} \sim 10\text{dB}$, proving the effectiveness of RSBUs in noise removal. As the noise decreases, the

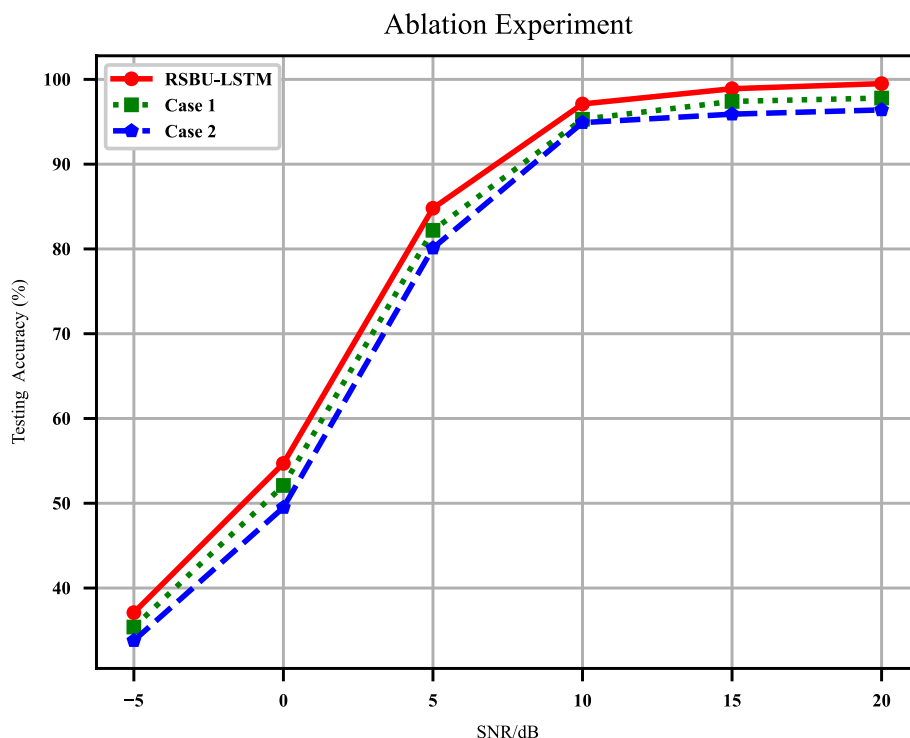


Fig. 5 Ablation experiment

identification accuracy of Case1 and Case2 tends to be consistent. The average identification accuracy of the proposed network has been improved by 2% and 3.6% compared to Case1 and Case2, respectively. Therefore, the better performance of the proposed network proves the effectiveness of the improvement.

4.3 Network performance and analysis

In the experiment, the MCLDNN [41], ResNet-LSTM [42], CLDNN [23], and ResNet18 [43] networks are selected for comparison with the proposed network. Figure 6 shows a comparison of the identification accuracy of 16 device signals from five networks when the SNR is $-5\text{dB} \sim 20\text{dB}$.

It can be seen from Fig. 6 that when the SNR is $-5\text{dB} \sim 20\text{dB}$, the identification accuracy of the five networks gradually increases with the increase in SNR, and the identification accuracy of the proposed network is always at the highest position. When the SNR is -5dB , the proposed network performance improvement is relatively clear. From Table 2, it can be seen that the proposed network has an average identification accuracy of 78.7% with a SNR of $-5\text{dB} \sim 20\text{dB}$, which is 2.2%, 4.7%, 6.3%, and 7% higher than the identification accuracy of MCLDNN, CLDNN, ResNet-LSTM, and ResNet18 networks, respectively. At lower SNR ($-5\text{dB} \sim 10\text{dB}$), the average identification accuracy of this network can reach 68.4%, which is 2.5%, 5.5%, 7.3%, and 8.2% higher than the identification accuracy of MCLDNN, CLDNN, ResNet-LSTM, and ResNet18 networks, respectively. Overall, the average identification accuracy of the proposed network is higher than the other four networks,

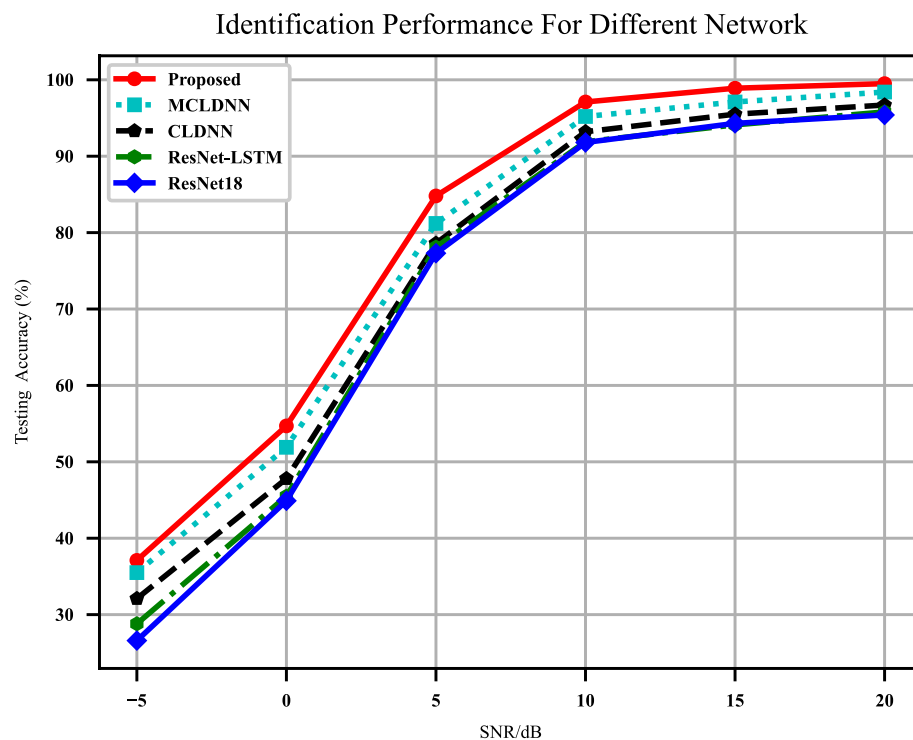


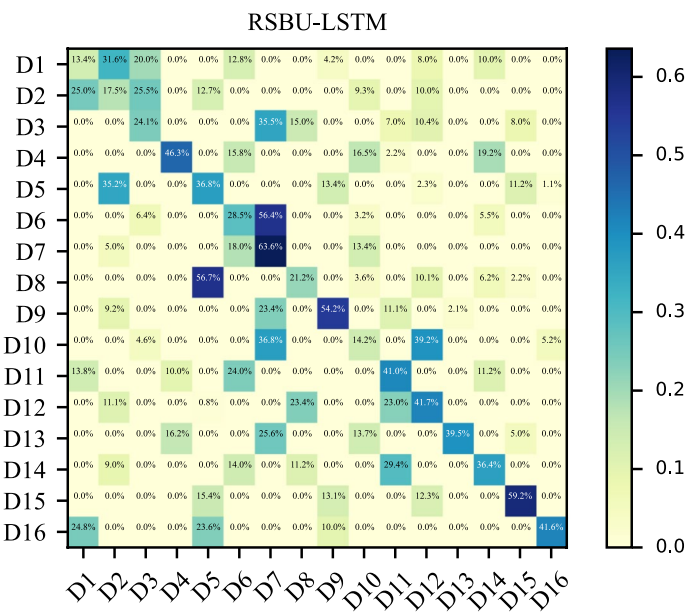
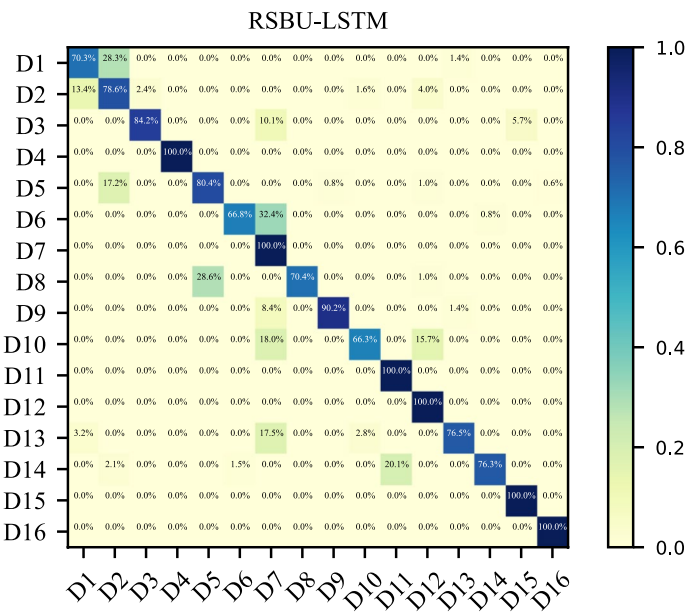
Fig. 6 Identification performance for different networks

Table 2 Average identification accuracy comparison

Network	-5dB (%)	0dB (%)	5dB (%)	10dB (%)	15dB (%)	20dB (%)
Proposed	37.1	54.7	84.8	97.1	98.9	99.5
MCLDNN	35.5	51.9	81.2	95.2	97.1	98.4
CLDNN	32.1	47.8	78.6	93.2	95.5	96.7
ResNet-LSTM	28.8	45.5	78.1	91.9	94.1	95.8
ResNet18	26.6	44.9	77.3	91.8	94.3	95.4

and the proposed network performance is the best. Subsequently, we use confusion matrices to analyze the identification performance of the network in detail.

Figures 7, 8 and 9 depict the overall confusion matrix of identification for RSBULSTM of -5dB , 5dB , and 20dB . At -5dB , some similar devices are difficult to identify due to the noise influence. At 5dB , there is a clear diagonal in the confusion matrix except for a few misclassified cases. At 20dB , except for a very small number of devices with identification deviations, it is basically possible to achieve full device identification. In general, the network has a good discrimination ability in low SNR environment.

**Fig. 7** Confusion matrix in -5dB**Fig. 8** Confusion matrix in 5dB

5 Conclusion

This paper proposes a RSBU-LSTM network relying on multiple features to achieve individual identification of wireless devices. In order to comprehensively utilize the feature information of signals, the RF signal is first divided into three data channel: I, Q, and phase. Considering that the signal contains a large amount of noise that affects feature extraction, we use multiple RSBUUs to suppress noise and extract the correlation features. Subsequently, the LSTM network was effectively combined with RSBUUs to achieve feature extraction within multiple signal cycles and between multiple signal

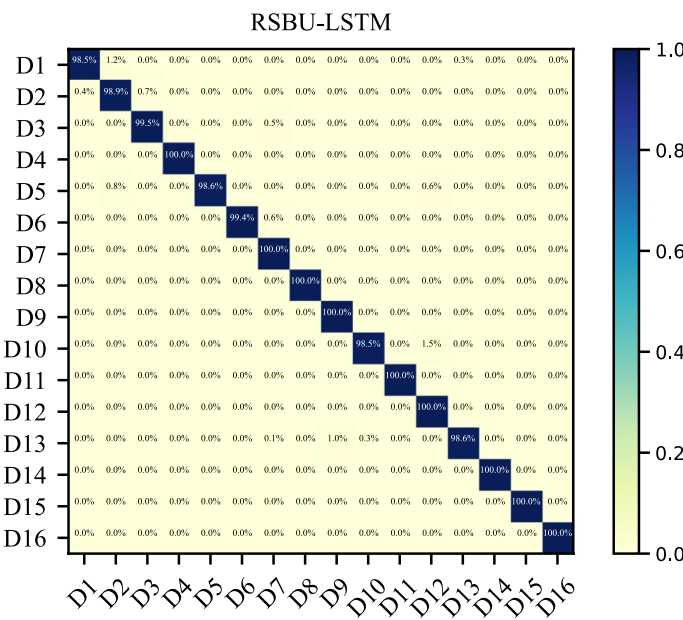


Fig. 9 Confusion matrix in 20dB

cycles. Finally, we concatenate all the features and then output the prediction results through the FC layer. Divide the open dataset into training and test sets, fully train the network through the training set, and use the test set to complete network testing. The experimental results show that the proposed network can effectively extract the RFFs of signals and accurately identify signals in low SNR environments. Compared with models based on 1D-ResNet and their improved versions, this network shows better performance. In the future, we will consider designing a network that utilizes unsupervised learning [44] to better extract signal features and utilize the new network to complete RFFI with limited samples under low SNR conditions.

Acknowledgements

Not applicable.

Author contribution

Haoran Ling conceived of the presented idea, developed the RFFI method based on RSBU-LSTM, discussed the results, and contributed to the final manuscript. Fengchao Zhu conceived of the presented idea, conducted the simulation experiments, verified the proposed methods, discussed the results, guided manuscript writing, and contributed to the final manuscript. Minli Yao conducted the simulation experiments, verified the proposed methods, discussed the results, and contributed to the final manuscript.

Funding

Funding was provided by General Program of National Natural Science Foundation of China (62071480).

Data availability

Available upon request.

Declarations

Competing interests

Not applicable.

Received: 29 January 2024 Accepted: 22 June 2024

Published online: 28 June 2024

References

- X. Huan, W. Chen, T. Wang, H. Hu, A microsecond energy-efficient LoRa time synchronization based on low-layer timestamping and asymmetric time translation. *IEEE Trans. Veh. Technol.* **73**, 1–6 (2023). <https://doi.org/10.1109/TVT.2023.3339169>
- F. Restuccia, S. D’Oro, T. Melodia, Securing the internet of things in the age of machine learning and software-defined networking. *IEEE Internet Things J.* **5**(6), 4829–4842 (2018). <https://doi.org/10.1109/JIOT.2018.2846040>
- O. Ureten, N. Serinken, Wireless security through RF fingerprinting. *Can. J. Electr. Comput. Eng.* **32**(1), 27–33 (2007). <https://doi.org/10.1109/CJCE.2007.364330>
- P. Scanlon, I.O. Kennedy, Y. Liu, Feature extraction approaches to RF fingerprinting for device identification in femto-cells. *Bell Labs Tech.* **15**(3), 141–151 (2010)
- S. Chen, F. Xie, Y. Chen, H. Song, H. Wen, Identification of wireless transceiver devices using radio frequency (RF) fingerprinting based on STFT analysis to enhance authentication security. *2017 IEEE 5th International Symposium on Electromagnetic Compatibility (EMC-Beijing)* (2017), p. 1–5. <https://doi.org/10.1109/EMC-B.2017.8260381>
- M. Lukacs, P. Collins, M. Temple, Classification performance using ‘RF-DNA’ fingerprinting of ultrawideband noise waveforms. *Electron. Lett.* **51**(10), 787–789 (2015)
- S. Chen, F. Xie, Y. Chen, H. Song, H. Wen, Identification of wireless transceiver devices using radio frequency (RF) fingerprinting based on STFT analysis to enhance authentication security. *2017 IEEE 5th International Symposium on Electromagnetic Compatibility (EMC-Beijing)* (2017), p. 1–5. <https://doi.org/10.1109/EMC-B.2017.8260381>
- G. Baldini, Radio frequency fingerprinting based on circulant singular spectrum analysis. *2022 International Symposium ELMAR* (2022), p. 85–90. <https://doi.org/10.1109/ELMAR55880.2022.9899714>
- X. Ouyang, L. Zhang, B. Gao, Research on radio station identification method based on combination of signal decomposition optimization and fractal processing. *2023 6th International Conference on Communication Engineering and Technology (ICCET), Xi'an, China, 2023* (2023), p 106–109
- Q. Wang, W. Tan, P. Li, X. Yan, H.-C. Wu, Y. Wu, Novel multiwavelet-based LPC random forest classifier for bluetooth RF-fingerprint identification. *2022 IEEE International Symposium on Broadband Multimedia Systems and Broadcasting (BMSB), Bilbao, Spain* (2022), p. 1–6
- Z. Chen, L. Peng, H. Fu, Isolated forest-based ZigBee device identification using adaptive filter coefficients. *2022 7th International Conference on Computer and Communication Systems (ICCCS), Wuhan, China* (2022), p. 715–720.
- W. Feng, Y. Li, C. Wu, J. Zhang, RF fingerprint extraction and device recognition algorithm based on multi-scale fractal features and APWOA-LSSVM. *EURASIP J. Adv. Signal Process.* **2023**(1), 131 (2023). <https://doi.org/10.1186/s13634-023-01098-9>
- X. Huan, Y. Hao, K. Miao, H. He, H. Hu, Carrier frequency offset in internet of things radio frequency fingerprint identification: an experimental review. *IEEE Internet Things J.* **11**(5), 7359–7373 (2024). <https://doi.org/10.1109/JIOT.2023.3328025>
- M. Nair, T. Cappello, S. Dang, V. Kalokidou, M.A. Beach, RF fingerprinting of LoRa transmitters using machine learning with self-organizing maps for cyber intrusion detection. *2022 IEEE/MTT-S International Microwave Symposium - IMS* (2022), p. 491–494. <https://doi.org/10.1109/IMS37962.2022.9865441>
- K. Merchant, S. Revay, G. Stantchev, B. Nousain, Deep learning for RF device fingerprinting in cognitive communication networks. *IEEE J. Sel. Top. Signal Process.* **12**(1), 160–167 (2018). <https://doi.org/10.1109/JSTSP.2018.2796446>
- S. Wang, L. Peng, H. Fu, A. Hu, X. Zhou, Convolutional neural network-based RF fingerprinting identification scheme for mobile phones. *IEEE INFOCOM 2020—IEEE Conference on Computer Communications Workshops (INFOCOM WKSHPS)* (2020), p. 115–120
- C. Li, J. Wang, W. Wang, H. Shi, RF-based on feature fusion and convolutional neural network classification of UAVs. *2022 IEEE 8th International Conference on Computer and Communications (ICCC), Chengdu, China* (2022), p. 1899–1904
- F. Chavez, B. Li, E. Cetin, Dual-layer waveform domain deep learning approach for RF fingerprinting. *2022 IEEE 65th International Midwest Symposium on Circuits and Systems (MWSCAS), Fukuoka, Japan* (2022), p. 1–5
- Z. Lu, T. Wang, X. Liu, N. Li, Deep learning based wireless device identification using RF fingerprint. *2023 3rd International Conference on Neural Networks, Information and Communication Engineering (NNICE), Guangzhou, China* (2023), p. 385–390
- J. Su, H. Liu, L. Yang, Specific emitter identification based on CNN via variational mode decomposition and bimodal feature fusion. *2023 IEEE 3rd International Conference on Power, Electronics and Computer Applications (ICPECA), Shenyang, China* (2023), p. 539–543
- W. Zhang, W. Zhao, X. Tan, L. Shao, C. Ran, Adaptive RF fingerprints fusion via dual attention convolutions. *IEEE Internet Things J.* **9**(24), 25181–25195 (2022). <https://doi.org/10.1109/JIOT.2022.3195736>
- G. Qing, H. Wang, T. Zhang, Radio frequency fingerprinting identification for Zigbee via lightweight CNN. *Phys. Commun.* **44**, 101250 (2021). <https://doi.org/10.1016/j.phycom.2020.101250>
- D. Jiao, Y. Peng, Y. Wang, J. Yang, Joint multislice and cooperative detection aided RFID method based on deep learning. *Phys. Commun.* **42**, 101153 (2020). <https://doi.org/10.1016/j.phycom.2020.101153>
- B. Li, E. Cetin, Waveform domain deep learning approach for RF fingerprinting. *2021 IEEE International Symposium on Circuits and Systems (ISCAS), Daegu, Korea* (2021), p. 1–5
- Y. Zhang, Y. Peng, B. Adebisi, G. Gui, H. Gacanin, H. Sari, Specific emitter identification based on radio frequency fingerprint using multi-scale network. *2022 IEEE 96th Vehicular Technology Conference (VTC2022-Fall)* (2022), p. 1–5. <https://doi.org/10.1109/VTC2022-Fall57202.2022.10013023>
- J. Li, Y. Ying, S. Wang et al., Slice combination convolutional neural network based radio frequency fingerprint identification for internet of things. *Wireless Netw.* **29**, 2953–2966 (2023). <https://doi.org/10.1007/s11276-023-03241-8>

27. X. Yan, Y. Chen, Q. Wang, H.-C. Wu, Y. Wu, Robust bluetooth RF-fingerprint identifier using wavelet scattering network. *2023 IEEE International Symposium on Broadband Multimedia Systems and Broadcasting (BMSB), Beijing, China* (2023), p. 1–5
28. J. Shi, et al., A radio frequency fingerprint identification method for wireless devices based on ShuffleNet-SVM. *2022 IEEE 8th International Conference on Computer and Communications (ICCC), Chengdu, China* (2022), pp. 1794–1800
29. Z. Chen, A.H.L. Peng et al., Generative adversarial network-based rogue device identification using differential constellation trace figure. *EURASIP J. Wirel. Commun. Netw.* **2021**, 72 (2021). <https://doi.org/10.1186/s13638-021-01950-2>
30. L. Chen, C. Zhao, Y. Zheng, Y. Wang, Radio frequency fingerprint identification based on transfer learning. *2021 IEEE/CIC International Conference on Communications in China (ICCC), Xiamen, China* (2021), pp. 81–85
31. X. Wang, Y. Zhang, H. Zhang et al., Radio frequency signal identification using transfer learning based on LSTM. *Circuits Syst Signal Process.* **39**, 5514–5528 (2020). <https://doi.org/10.1007/s00034-020-01417-7>
32. J. Zhou, Y. Peng, G. Gui, Y. Lin, B. Adebisi, H. Gacanin, H. Sari, A novel radio frequency fingerprint identification method using incremental learning. *2022 IEEE 96th Vehicular Technology Conference (VTC2022-Fall), London, United Kingdom* (2022), p. 1–5
33. N. Yang, B. Zhang, G. Ding, Y. Wei, G. Wei, J. Wang, D. Guo, Specific emitter identification with limited samples: a model-agnostic meta-learning approach. *IEEE Commun. Lett.* **26**(2), 345–349 (2022). <https://doi.org/10.1109/LCOMM.2021.3110775>
34. G. Reus-Muns, K.R. Chowdhury, Classifying UAVs with proprietary waveforms via preamble feature extraction and federated learning. *IEEE Trans. Veh. Technol.* **70**(7), 6279–6290 (2021). <https://doi.org/10.1109/TVT.2021.3081049>
35. W. Wu, S. Hu, D. Lin, Z. Liu, Dsln: securing internet of things through RF fingerprint recognition in low-SNR settings. *IEEE Internet Things J.* **9**(5), 3838–3849 (2022). <https://doi.org/10.1109/JIOT.2021.3100398>
36. B. Wang, Y.S.Z. Jiang, otyhers: an intelligent signal processing method against impulsive noise interference in AoT. *EURASIP J. Adv. Signal Process.* **2023**(1), 104 (2023). <https://doi.org/10.1186/s13634-023-01061-8>
37. S. Riyaz, K. Sankhe, S. Ioannidis, K. Chowdhury, Deep learning convolutional neural networks for radio identification. *IEEE Commun. Mag.* **56**(9), 146–152 (2018). <https://doi.org/10.1109/MCOM.2018.1800153>
38. M. Zhao, S. Zhong, X. Fu, B. Tang, M. Pecht, Deep residual shrinkage networks for fault diagnosis. *IEEE Trans. Ind. Inform.* **16**(7), 4681–4690 (2020). <https://doi.org/10.1109/TII.2019.2943898>
39. S. Hochreiter, J. Schmidhuber, Long short-term memory. *Neural Comput.* **9**(8), 1735–1780 (1997). <https://doi.org/10.1162/neco.1997.9.8.1735>
40. K. Sankhe, M. Belgiovine, F. Zhou, S. Riyaz, S. Ioannidis, K. Chowdhury, Oracle: optimized radio classification through convolutional neural networks. *IEEE INFOCOM 2019—IEEE Conference on Computer Communications* (2019), p. 370–378. <https://doi.org/10.1109/INFOCOM.2019.8737463>
41. J. Xu, C. Luo, G. Parr, Y. Luo, A spatiotemporal multi-channel learning framework for automatic modulation recognition. *IEEE Wirel. Commun. Lett.* **9**(10), 1629–1632 (2020). <https://doi.org/10.1109/LWC.2020.2999453>
42. A. Mohammad, M. Ashraf, M. Valkama, B. Tan, Learning-based RF fingerprinting for device identification using amplitude-phase spectrograms. *2023 IEEE 98th Vehicular Technology Conference (VTC2023-Fall)* (2023), p. 1–6. <https://doi.org/10.1109/VTC2023-Fall60731.2023.10333639>
43. H.-K. Le, V.-P. Hoang, V.-S. Doan, M.-T. Hoang, N.P. Dao, Performance analysis of convolutional neural networks with different window functions for automatic modulation classification. *2022 13th International Conference on Information and Communication Technology Convergence (ICTC)* (2022), p. 153–157. <https://doi.org/10.1109/ICTC55196.2022.9952750>
44. C. Wang, S. Wu, X. Shao, Unsupervised domain adaptive bearing fault diagnosis based on maximum domain discrepancy. *EURASIP J. Adv. Signal Process.* **2024**(11), 1–19 (2024). <https://doi.org/10.1186/s13634-023-01107-x>

Publisher's Note

Springer Nature remains neutral with regard to jurisdictional claims in published maps and institutional affiliations.